Inorg. Chem. **2006**, *45*, 8965–8972

Structural, Thermal, Spectroscopic, Specific-Heat, and Magnetic Studies of $(C_5H_{18}N_3)[Fe_3(HPO_3)_6]\cdot 3H_2O$: A New Organically Templated Iron(III) Phosphite with a Pillared Structure Formed by the Interpenetration of Two Subnets

U.-Chan Chung,[†] José L. Mesa,*[,‡] José L. Pizarro,[†] Jesús Rodríguez Fernández,[§] Jorge Sánchez Marcos,[§] José S. Garitaonandia,[||] María I. Arriortua,[†] and Teófilo Rojo[‡]

Departamento de Mineralogía y Petrología, Departamento de Química Inorgánica, and Departamento de Física Aplicada II, Facultad de Ciencia y Tecnología, Universidad del País Vasco, Apdo. 644, E-48080 Bilbao, Spain, and CITIMAC, Facultad de Ciencias, Universidad de Cantabria, Avenida los Castros, 39005 Santander, Spain

Received May 12, 2006

A new open framework iron(III) phosphite with formula $(C_5H_{18}N_3)[Fe_3(HPO_3)_6]\cdot 3H_2O$ has been prepared by hydrothermal synthesis with *N*-(2-aminoethyl)-1,3-propanediamine as a templating agent. The crystal structure was solved from single-crystal X-ray diffraction data in the trigonal space group $R\bar{3}$. The unit cell parameters are $a = 8.803(1)$ Å and $c = 25.292(2)$ Å with $Z = 3$. The complex pillared structure can be described as two interpenetrating subnets, one organic, $[(C_5H_{18}N_3)\cdot 3H_2O]^{3+}$, and one inorganic, $[Fe_3(HPO_3)_6]^{3-}$. In the inorganic subnet, the pillars are formed by FeO_6 trimers linked by vertex sharing phosphite groups, while in the cationic subnet the organic molecules act like pillars. With increasing temperature, the flexibility of the structure allows contraction due to dehydration followed by thermal expansion before reaching the thermal stability limit. The *Dq* and Racah parameters calculated for $(C_5H_{18}N_3)[Fe_3(HPO_3)_6]\cdot 3H_2O$ are $Dq = 965$, $B = 1080$, and $C = 2472$ cm^{-1}. Mössbauer spectroscopy confirms the trivalent oxidation state of iron cations and the crystallographic multiplicities of their sites. The ESR spectra show isotropic signals with a *g*-value of 2.00(1). Specific-heat measurements show a three-dimensional (λ-type) peak at a critical temperature $T_c = 32$ K. The value of the entropy at saturation is 46 J/mol K, very near the expected value of 44.7 J/mol K for the iron(III) cations with $S = {}^5/_2$. Magnetic measurements indicate a three-dimensional antiferromagnetic ordering below 32 K and a reorientation of spins below 15 K with an incomplete cancellation of spins due to triangular interactions inherent to the structure.

Introduction

Open framework inorganic−organic materials are of significant interest due to their potential as precursors for microporous materials. The great number of metal cations that can be used to obtain these compounds makes it possible to have potential applications in numerous fields, such as catalysis, biological systems, and electromagnetic and optical functions.[1] The phosphate group, $(PO_4)^{3-}$, has historically been one of the most productive oxo-anions for obtaining new structures,[1c,2] but the chemical diversity of related materials includes arsenates,[3] sulfates,[4] germanates,[5] carbonates,[6] selenites, and so forth.[7]

* Corresponding author: E-mail: joseluis.mesa@ehu.es; Phone: +34 94 6015523; Fax: +34 94 6013500.
[†] Departamento de Mineralogía y Petrología, Universidad del País Vasco.
[‡] Departamento de Química Inorgánica, Universidad del País Vasco.
[§] Universidad de Cantabria.
[||] Departamento de Física Aplicada II, Universidad del País Vasco.

(1) (a) Ferey, G. *Chem. Mater*. **2001**, *13*, 3048. (b) Eddaoudi, M.; Moler, D. B.; Li, H.; Chen, B.; Reineke, T. M.; O'Keefe, M.; Yaghi, O. M. *Acc. Chem Res*. **2001**, *34*, 319. (c) Cheetham, A. K.; Ferey, G.; Loiseau, T. *Angew. Chem., Int. Ed.* **1999**, *38*, 3268. (d) Hagrman, P. J.; Hagrman, D.; Zubieta, J. *Angew. Chem., Int. Ed*. **1999**, *38*, 2638.
(2) (a) Rao, C. N. R. *Indian J. Chem., Sect. A* **2003**, *42A*, 2163. (b) Finn, R. C.; Zubieta, J.; Haushalter, R. C. *Prog. Inorg. Chem*. **2003**, *51*, 421. (c) Boudin, S.; Guesdon, A.; Leclaire, A.; Borel, M. M. *Int. J. Inorg. Mater*. **2000**, *2*, 561.
(3) (a) Bazán, B.; Mesa, J. L.; Pizarro, J. L.; Lezama, L.; Arriortua, M. I.; Rojo, T. *Inorg. Chem*. **2000**, *39*, 6056. (b) Yang, G.; Li, L.; Chen, J.; Xu, R. *J. Chem. Soc., Chem. Commun*. **1989**, *13*, 810. (c) Chen, J.; Xu, R. *J. Solid State Chem*. **1989**, *80*, 149.
(4) (a) Behera, J. N.; Gopalkrishnan, K. V.; Rao, C. N. R. *Inorg. Chem*. **2004**, *42*, 2636. (b)Bataille, T.; Louer, D. *J. Mater. Chem*. **2002**, *12*, 3487.

10.1021/ic060815u CCC: $33.50
Published on Web 09/27/2006

In recent years, the phosphite group, $(HPO_3)^{2-}$, has been the source of numerous organically templated structures. In this oxo-anion, the phosphorus remains in a low oxidation state, +3, and the group has pyramidal morphology, which opens the range of possibilities to obtain new structural species, the versatility of this group allowing it to build either open or condensed frameworks.[8] Since the first organically templated phosphite was synthesized,[9] this family of compounds has grown rapidly, especially those in which the transition metal cation is zinc.[10] Open framework phosphites of vanadium,[11] manganese,[12] cobalt,[13] iron,[14] chromium,[15] gallium,[16] and even indium[17] have been prepared, but they are still less numerous than those reported with Zn.

As iron phosphates are one of the most important groups of open framework transition metal compounds, iron was chosen as an ideal candidate in order to obtain new organically templated phosphites with interesting properties. We present in this paper the synthesis, characterization, and physical properties of a new iron(III) phosphite, templated with *N*-(2-aminoethyl)-1,3-propanediamine, which exhibits a complex pillared structure formed by the interpenetration of two subnets and a complex magnetic behavior.

Experimental Section

Synthesis and Characterization. $(C_5H_{18}N_3)[Fe_3(HPO_3)_6]\cdot 3H_2O$ has been synthesized using mild hydrothermal conditions and autogenous pressure. H_3PO_3 (12 mmol) and $Fe(SO_4)_3\cdot 5H_2O$ (0.16 mmol) were dissolved in distilled water (20 mL), and *N*-(2-aminoethyl)-1,3-propanediamine (23 mmol) was added to the solution while stirring. A 10 mL portion of an organic cosolvent (butanol) was also added. The pH of the solution was 5. The solution was sealed in a PTFE-lined steel pressure vessel which, after 5 days at 170 °C, was slowly cooled to room temperature. Colorless crystals were separated by filtering, washed with water and acetone, and dried in air. The yield of the reaction was approximately 65% based on iron content.

The density was measured by the flotation method using a mixture of bromoform (Br_3CH, $\rho = 2.82$ g·cm^{-3}) and chloroform (Cl_3CH, $\rho = 1.476$ g·cm^{-3}), obtaining an experimental density, ρ_{exp}, of 2.38(4) g·cm^{-3}.

Iron and phosphorus contents were measured by inductively coupled plasma atomic emission spectroscopy (ICP-EAS) while carbon, nitrogen, and hydrogen contents were measured by elemental analysis. The obtained values are Fe, 19.7%; P, 22.0%; C, 7.2%; N, 5.0%; and H, 2.9% (required Fe, 20.4%; P, 22.6%; C, 7.3%; N, 5.1%; and H, 3.6%).

The infrared spectrum of $(C_5H_{18}N_3)[Fe_3(HPO_3)_6]\cdot 3H_2O$ shows the characteristic bands of the protonated aminoethylpropanediamine (3020−2850 cm^{-1}), the water molecules (3400, 1600 cm^{-1}), and the phosphite oxoanion (1050, 985, 630, and 500 cm^{-1}). A single P−H stretching band at 2465 cm^{-1} indicates the presence of a crystallographically independent phosphite group in the structure. The positions of the bands of both the organic molecule and phosphite oxoanion are similar to those reported in the literature.[18]

Crystal Structure Determination. A single crystal with dimensions 0.05 × 0.03 × 0.02 mm^3 was selected under a polarizing microscope and mounted on a glass fiber. Single-crystal X-ray diffraction data were collected at room temperature on an Oxford Diffraction XCALIBUR2 automated diffractometer (Mo Kα radiation) equipped with a CCD detector. The diffractometer software[19] was used to make the Lorentz polarization and absorption corrections, taking into account the size and shape of the crystal, as well as the data reduction. There were 5437 reflections measured during data collection of which 1104 were unique with an R_{int} factor of 4.65%. The number of observed reflections with $I > 2\sigma(I)$ was 808. The structure was solved by direct methods using SHELXS 97[20] in the $R\bar{3}$ space group. SHELXL 97[21] was used to refine the structure by least-squares based on F^2. All the atoms belonging to the inorganic framework were initially located except the hydrogens of the phosphite group. Carbon and nitrogen atoms were definitely assigned while refining the structure. The organic and water molecules were present in a dynamic disorder that made it impossible to geometrically place the hydrogen atoms belonging

(5) (a) Julius, N. N.; Choudhury, A.; Rao, C. N. R. *J. Solid State Chem.* **2003**, *170*, 124. (b) Beitone, L.; Loiseau, T.; Ferey, G. *Inorg. Chem.* **2002**, *41*, 3962.

(6) Harrison, W. T. A.; Phillips, M. L. F.; Nenoff, T. M.; MacLean, E. J.; Teat, S. J.; Maxwell, R. S. *J. Chem. Soc., Dalton Trans.* **2001**, *5*, 546.

(7) (a) Udayakumar, D.; Rao, C. N. R. *J. Mater. Chem.* **2003**, *13*, 1635. (b) Pasha, I.; Choudhury, A.; Rao, C. N. R. *Solid State Sci.* **2003**, *5*, 257.

(8) (a) Corbridge, D. E. C. *Acta Crystallogr.* **1956**, *9*, 991. (b) Marcos, M. D.; Amoros, P.; Beltrán-Porter, A.; Martinez-Manez, R.; Attfield, M. P. *Chem. Mater.* **1993**, *5*, 121. (c) Foulon, J. D.; Tijani, N.; Durand, J.; Rafiq, M.; Cot, L. *Acta Crystallogr.* **1993**, *C49*, 1. (d) Morris, R. E.; Attfield, M. P.; Cheetham, A. K. *Acta Crystallogr.* **1994**, *C50*, 473. (e) Ewald, B.; Prots, Y.; Kniep, R. *Z. Kristallogr.*—New Cryst. Struct. **2003**, *218*, 377. (f) Chung, U.-C.; Mesa, J. L.; Pizarro, J. L.; Jubera, V.; Lezama, L.; Arriortua, M. I.; Rojo, T. *J. Solid State Chem.* **2005**, *178*, 2913.

(9) Bonavia, G.; DeBord, J.; Haushalter, R. C.; Rose, D.; Zubieta, J. *Chem. Mater.* **1995**, *7*, 1995.

(10) (a) Johnstone, J. A.; Harrison, W. T. A. *Inorg. Chem.* **2004**, *43*, 4567. (b) Fu, W. S.; Shi, Z.; Li, G. N.; Zhang, D.; Dong, W. J.; Chen, X. B.; Feng, S. H. *Solid State Sci.* **2004**, *6*, 225. (c) Liang, J.; Wang, Y.; Yu, J. H.; Li, Y.; Xu, R. R. *Chem. Commun.* **2003**, *7*, 882. (d) Harrison, W. T. A.; Phillips, M. L. F.; Stranchfield, J.; Nenoff, T. M. *Inorg. Chem.* **2001**, *40*, 895. (e) Rodgers, J. A.; Harrison, W. T. A. *Chem. Commun.* **2000**, *23*, 2385. (f) Wang, Y.; Yu, J. H.; Du, Y.; Shi, Z.; Zou, Y. C.; Xu, R. R. *J. Chem. Soc., Dalton Trans.* **2002**, *21*, 4060.

(11) (a) Shi, Z.; Zhang, D.; Li, G. H.; Wang, L.; Lu, X. Y.; Hua, J.; Feng, S. H. J. *Solid State Chem.* **2003**, *172*, 464. (b) Harrison, W. T. A. *Solid State Sci.* **2003**, *5*, 297. (c) Shi, Z.; Li, G. H.; Zhang, D.; Hua, J.; Feng, S. H. *Inorg. Chem.* **2003**, *42*, 2357. (d) Fernandez, S.; Mesa, J. L.; Pizarro, J. L.; Lezama, L.; Arriortua, M. I.; Rojo, T. *Chem. Mater.* **2003**, *15*, 1204. (e) Fernandez, S.; Mesa, J. L.; Pizarro, J. L.; Lezama, L.; Arriortua, M. I.; Rojo, T. *Chem. Mater.* **2002**, *14*, 2300.

(12) Fernandez, S.; Mesa, J. L.; Pizarro, J. L.; Lezama, L.; Arriortua, M. I.; Olazcuaga, R.; Rojo, T. *Chem. Mater.* **2000**, *12*, 2092.

(13) Fernandez, S.; Mesa, J. L.; Pizarro, J. L.; Lezama, L.; Arriortua, M. I.; Rojo, T. *Int. J. Inorg. Mater.* **2001**, *3*, 331.

(14) (a) Fernandez, S.; Mesa, J. L.; Pizarro, J. L.; Lezama, L.; Arriortua, M. I.; Rojo, T. *Chem. Mater.* **2002**, *14*, 2300. (b) Fernandez-Armas, S.; Mesa, J. L.; Pizarro, J. L.; Garitaonandia, J. S.; Arriortua, M. I.; Rojo, T. *Angew. Chem., Int. Ed.* **2004**, *43*, 977. (c) Chung, U.-C.; Mesa, J. L.; Pizarro, J. L.; Lezama, L.; Garitaonandia, J. S.; Chapman, J. P.; Arriortua, M. I. J. *Solid State Chem.* **2004**, *177*, 2705. (d) Mandal, S.; Pati, S. K.; Green, M. A.; Natarajan, S. *Chem. Mater.* **2005**, *17*, 638.

(15) Fernandez, S.; Mesa, J. L.; Pizarro, J. L.; Lezama, L.; Arriortua, M. I.; Rojo, T. *Angew. Chem., Int. Ed.* **2002**, *41*, 3683.

(16) Fernandez-Armas, S.; Mesa, J. L.; Pizarro, J. L.; Lezama, L.; Arriortua, M. I.; Rojo, T. *J. Solid State Chem.* **2004**, *177*, 765.

(17) Yi, Z.; Chen, C.; Li, S.; Li, G.; Meng, H.; Cui, Y.; Yang, Y.; Pang, W. *Inorg. Chem. Commun.* **2005**, *8*, 166.

(18) (a) Gharbi, A.; Jouini, A.; Averbuch-Pouchot, M. T.; Durif, A. *J. Solid State Chem.* **1994**, *111*, 330. (b) Fernandez, S.; Mesa, J. L.; Pizarro, J. L.; Lezama, L.; Arriortua, M. I.; Olazcuaga, R.; Rojo, T. *Inorg. Chem.* **2001**, *40*, 3476.

(19) *CRYSALIS*, version 1.170.32; Oxford Diffraction Ltd.: Oxford, 2003.

(20) Sheldrick, G. M. *SHELXS97 Program for the solution of crystal structures*; University of Göttingen: Göttingen, Germany, 1997.

(21) Sheldrick, G. M. *SHELXS97 Program for the refinement of crystal structures*; University of Göttingen: Göttingen, Germany, 1997.

Table 1. Crystallographic Data for $(C_5H_{18}N_3)[Fe_3(HPO_3)_6]\cdot 3H_2O$

chemical formula	$(C_5H_{18}N_3)[Fe_3(HPO_3)_6]\cdot 3H_2O$
fw, g·mol^{-1}	821.69
space group	$R\bar{3}$ (No. 148)
a, Å	8.803(1)
c, Å	25.292(2)
g, deg.	120
V, Å^3	*1697.4(3)*
Z	3
ρ_{obs}, ρ_{calc}, g·cm^{-3}	2.38(4), 2.412
T, K	298
radiation, λ(Mo Kα), Å	0.7107
μ (Mo Kα), mm^{-1}	2.430
R [$I > 2\sigma(I)$][a]	R1=0.0349, wR2=0.0674
R [all data]	R1=0.0715, wR2=0.0768

[a] $R1 = \sum||F_o| - ||F_c||/\sum|F_o|$; $wR2 = [\sum w(|F_o| - |F_c|)^2/\sum w|F_o|^2]^{1/2}$; $w = 1/[\sigma^2|F_o|^2 + (0.031P)^2]$, where $P = [\text{Max}|F_o|^2 + 2|F_c|^2/3$.

Table 2. Selected Bond Distances (Å) and Angles (deg)[a]

Bond Distances	
$Fe(1)O_6$ Octahedron	
Fe(1)−O(2)	2.025(2)
Fe(1)−O(2)^{i,ii}	2.025(2)
Fe(1)−O(3)	1.999(2)
Fe(1)−O(3)^{i,ii}	1.999(2)
$Fe(1)O_6$ Octahedron	
Fe(2)−O(1)	2.010(2)
Fe(2)−O(1)^{iii,iv,v,vi,vii}	2.010(2)
HPO_3 Pyramid	
P−O(1)	1.526(3)
P−O(2)	1.530(3)
P−O(3)^{viii}	1.526(3)
P−H	1.20(2)

[a] Symmetry codes: i = $-x + y + 1, -x + 1, z$; ii = $-y + 1, x - z, z$; iii = $-x + y, -x + 1, z$; iv = $x - y + {}^2/_3, x + {}^1/_3, -z + {}^1/_3$; v = $-y + 1, x - y + 1, z$; vi= $-x + {}^2/_3, -y + {}^4/_3, -z + {}^1/_3$; vii = $y + {}^1/_3, -x + y + {}^1/_3, -z + {}^1/_3$; viii = $-x + 1, -y + 1, -z$.

to them. All the atoms, except the hydrogens of the phosphite group, were anisotropically refined. The final *R*-factors were R1= 0.0715 and wR2= 0.0768 for all data. Crystallographic data and selected bond distances are listed in Tables 1 and 2, respectively. Atomic coordinates are given as Supporting Information.

Physicochemical Characterization Techniques. The IR spectrum was recorded using KBr pellets, within the 400−4000 cm^{-1} region on a Mattson FTIR 1000 spectrometer. Thermogravimetric analysis was carried out in a SDC 2960 simultaneous DSC-TGA instrument, under a synthetic air atmosphere, from room temperature to 800 °C. Temperature-dependent X-ray diffraction studies were performed in a Philips X'Pert automatic diffractometer (Cu Kα radiation) equipped with a variable-temperature Anton Paar HTK16 Pt stage. The diffuse reflectance spectrum from 210 to 2000 nm was obtained with a CARY 5000 UV−vis-IR spectrometer. The Mössbauer spectra were fitted with the NORMOS[22] program using α-Fe as reference to evaluate the isomer shift. A Bruker ESP 300 spectrometer was used to record the ESR spectra between 290 and 4.2 K. The temperature was stabilized by an Oxford Instrument (ITC 4) regulator. Heat capacity measurements were carried out by a two-τ relaxation method, using a PPMS-system, with magnetic fields up to 9 T and temperatures down to 2 K. Magnetic measurements on a powdered sample were performed in the temperature range 5−300 K, using a Quantum Design MPMS-7 SQUID magnetometer, under 1000 and 100 G applied magnetic fields, values in the range of linear dependence of magnetization versus magnetic field, even at 5 K.

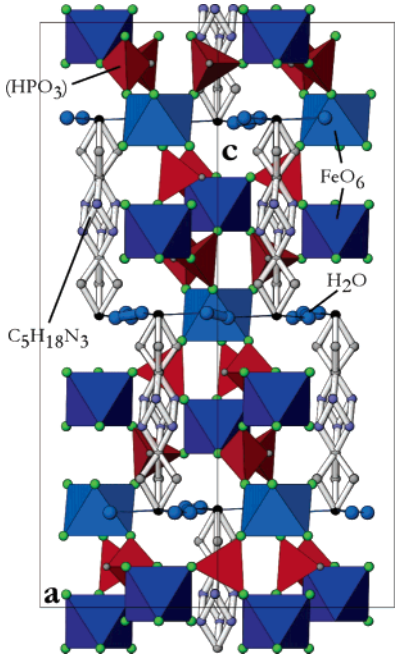

Figure 1. View of the complex structure of $(C_5H_{18}N_3)[Fe_3(HPO_3)_6]\cdot 3H_2O$.

Results and Discussion

Crystal Structure Description. The structure of $(C_5H_{18}N_3)[Fe_3(HPO_3)_6]\cdot 3H_2O$ consists of a complex, pillared, three-dimensional framework (Figure 1) that can be described as two interpenetrating subnets, one organic and the other inorganic. The inorganic subnet, $[Fe_3(HPO_3)_6]^{3-}$, is composed of FeO_6 octahedra interconnected by phosphite groups, $(HPO_3)^{2-}$, forming trimeric units where Fe(1) atoms are located in the extremes and Fe(2) in the middle. This organization presents a clear resemblance with the NASICON structure.[23] In the same trimer, the linkage between $Fe(1)O_6$ and $Fe(2)O_6$ octahedra is made by three phosphite groups, and the distance between the terminal irons, Fe(1), is 9.55 Å. Considering the trimers as pillars, it can be seen that each pillar is connected via phosphite groups to another six (three at each end) forming an open subnet with honeycomb-like levels of Fe(1). The organic molecules can be considered as pillars which connect to other six (three at each end) via water molecules and forming another open subnet. The organic subnet, $[(C_5H_{18}N_3)\cdot 3H_2O]^{3+}$, is structurally equivalent to the inorganic one. The organic molecules present rotational disorder around the −3 axis. This disorder causes the splitting of C(1), N(2), and C(3) in three positions each. N(3) and C(3) occupy the same sites with a statistical distribution of 50% reducing their occupation factor to $^1/_6$ each as they occupy six positions. C(1) has an occupation factor of $^1/_3$ while it is occupying three positions. This effect produces various possible configurations of the organic molecules. Something similar occurs with the water molecule's oxygen, with the consequent splitting in two posi-

(22) Brand, R. A.; Lauer, J.; Herlach, D. M. *J. Phys. F: Met. Phys.* **1983**, *13*, 675.

(23) Chakir, M.; Jazouli, A. El.; de Waal, D. *Mater. Res. Bull.* **2003**, *38*, 1773.

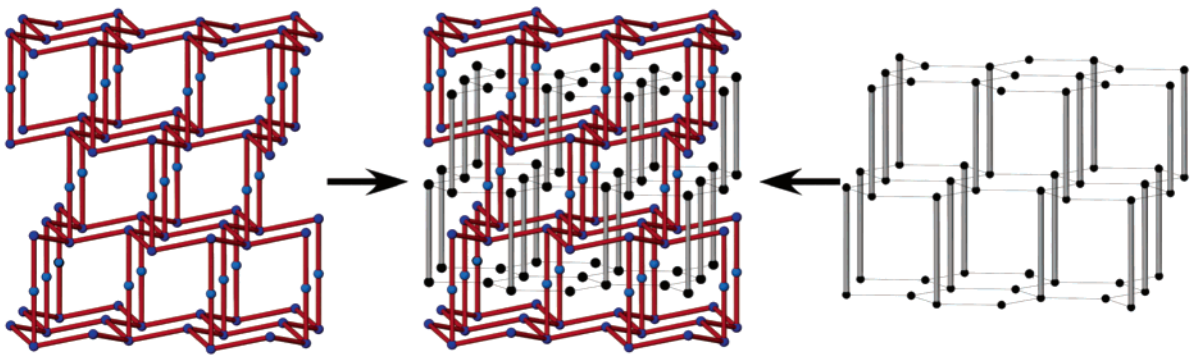

Figure 2. Interpenetration of both inorganic and organic subnets giving rise to the complete structure of $(C_5H_{18}N_3)[Fe_3(HPO_3)_6]\cdot 3H_2O$.

tions. The pillars in this subnet are formed by the organic cations which link between them by the terminal nitrogens via water molecules by hydrogen bonds, building up the organic subnet. The length of the organic molecules is 8.44 Å. As both organic and inorganic subnets are open, the interpenetration of one into the other takes place with the trimer pillars occupying the hollows of the organic subnet and vice versa (Figure 2).

The iron atoms occupy two different crystallographic sites with Fe(1)/Fe(2) ratio of 2:1, and the phosphorus is located in a general site. The Fe(1) links to three O(3) with a bond distance of 1.999(2) Å, and to three O(2) with a bond distance of 2.025(2) Å. The cis O−Fe(1)−O angles range from 88.81(9)° to 90.89(9)°, and the trans angles are 178.4(1)°. The Fe(2) links to six O(1) with a bond distance of 2.010(2) Å. The coordination polyhedron of Fe(2) has cis O−Fe−O angles between 87.63(9)° and 92.37(9)° while the trans angles are 180°. The bond distances of the phosphite group are between 1.527(2) and 1.530(2) Å for P−O bonds, and are 1.17(3) Å for the P−H bond. The angles of this anionic group vary between 110.1(1)° and 112.1(1)° for O−P−O, and between 104(2)° and 112(2)° for O−P−H.

Distortion calculations were made for the Fe coordination polyhedra compared to the ideal geometries of polyhedra with coordination number 6 (octahedron and trigonal prism), using the model proposed by Muetterties and Guggenberger.[24] In this model, real and ideal polyhedra are compared by evaluating their dihedral angles. The results confirmed the high regularity of both $Fe(1)O_6$ and $Fe(2)O_6$ octahedra with distortions of 7.7% and 1.4%, respectively. Brown and Altermatt's bond valence calculations,[25] in which an ion's valence is estimated from the bond distances, were made using the formula $s = \exp[(r_0 - r)/B]$ where r_0 (1.79 Å) and B (0.37 Å) are empirical values reported in the literature[26] and r is the experimental bond distance. As there are no tabulated bond distances for phosphorus in oxidation state +3, $(PH)^{4+}$ groups have been considered using $r_0 = 1.626$ Å and $B = 0.37$ Å.[27] The results, Fe(1), 3.0 v.u.; Fe(2), 3.04 v.u.; $(PH)^{4+}$, 3.9 v.u.; O(1), 1.81 v.u.; O(2), 1.78 v.u.; O(3), 1.83 v.u., are in good agreement with the oxidation states of the Fe^{3+} and $(PH)^{4+}$ groups while the oxygens show a ca. 0.2 deficit caused by hydrogen bond type interactions.

Thermal Behavior. The TG curve shows a rapid mass loss, 4%, between room temperature and 90 °C due to the dehydration of the phase. This process continues with the loss of another 3% of mass, from 90 to 280 °C, the temperature after which the TG curve descends more rapidly up a temperature of 700 °C. The sharp peak at 290 °C in the DTA curve marks the exothermic process of calcination of the organic molecules. Between 700 and 800 °C, there is a mass gain from 76% to 77% due to oxidation processes to form the high-temperature residual phases.

Temperature-dependent X-ray diffraction patterns show that the thermal stability limit of $(C_5H_{18}N_3)[Fe_3(HPO_3)_6]\cdot 3H_2O$ is 270 °C, the temperature at which the structure starts to collapse due to the calcination of the organic molecule. A closer look at the diffraction patterns (Figure 3) reveals a thermal evolution of the cell parameters with a volume reduction of, approximately, 50 $Å^3$ between room temperature and 100 °C due to the dehydration of the compound. From 100 °C the cell volume starts to increase reaching a maximum gain of 15 $Å^3$ at 270 °C. This thermal expansion is possible because of the flexibility of the structure.

UV−Vis and Mössbauer Spectroscopies. In the diffuse reflectance spectrum of $(C_5H_{18}N_3)[Fe_3(HPO_3)_6]\cdot 3H_2O$ (see Supporting Information), characteristic bands belonging to Fe^{3+} are present. These bands correspond to the forbidden transitions of a d^5 high spin configuration cation from the ground level $^6A_{1g}(^6S)$ to the excited $^4T_{1g}(^4G)$ [780 nm]; $^4T_{2g}(^4G)$ [565 nm]; $^4A_{1g}(^4G)$, $^4E_g(^4G)$ [430 nm] and $^4T_{2g}(^4D)$ [380 nm] levels. The Racah, $B = 1080$ cm^{-1}, $C = 2472$ cm^{-1}, and $Dq = 965$ cm^{-1}, parameters have been calculated, showing minimal covalent character since the B-value is approximately 94% of that corresponding to the free ion (1150 cm^{-1}).[28]

The Mössbauer spectrum of $(C_5H_{18}N_3)[Fe_3(HPO_3)_6]\cdot 3H_2O$ (Figure 4) shows, in the paramagnetic region, 300 K to, approximately, 35 K, a signal composed of two symmetric

(24) Muetterties, E. L.; Guggenberger, L. J. *J. Am. Chem. Soc*. **1974**, *96*, 1748.
(25) Brown, I. D.; Altermatt, D. *Acta Crystallogr*. **1985**, *B41*, 244.
(26) Brese, N. E.; O'Keeffe, M. *Acta Crystallogr*. **1991**, *B47*, 192.
(27) Loub, J. *Acta Crystallogr*. **1991**, *B47*, 468.
(28) Lever, A. B. P. *Inorganic Electronic Spectroscopy*; Elsevier Science Publishers B. V.: Amsterdam, Netherlands, 1984.

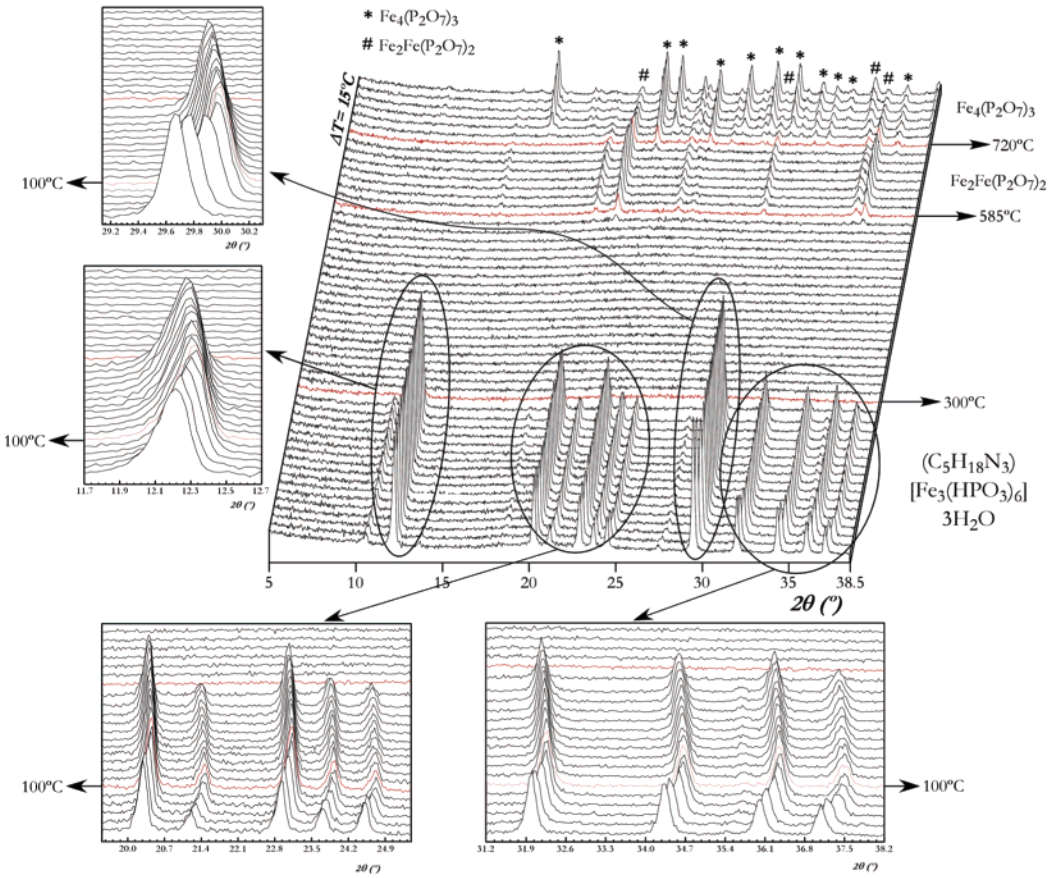

Figure 3. Temperature-dependent X-ray diffraction patterns showing thermal stability limit and the cell volume variation with temperature.

doublets corresponding to the iron cations, characteristic of purely electrostatic interactions. The values of isomer shift [0.39(1), 0.53(1) mm s^{-1} for Fe(1) and Fe(2), respectively] and quadrupolar splitting [0.24(1) mm s^{-1} for both Fe(1) and Fe(2)] are typical of Fe(III) ions in highly symmetric octahedral coordination.[29] The 2:1 ratio of the spectral areas corresponding to Fe(1) and Fe(2), respectively, were fixed to this ratio before the fit of the spectra and agree well with the crystallographic multiplicities of their positions.

In the magnetic ordered region, approximately from 30 to 12 K, the Mössbauer signals corresponding to the crystallographically independent $Fe(1)O_6$ and $Fe(2)O_6$ sublattices are split in two sextuplets due to the Zeeman effect. The hyperfine field values below 35 K show differences between those corresponding to Fe(1) and Fe(2) sites and increase with decreasing temperature from 22.54(2) and 33.19(3) T for Fe(1) and Fe(2) sites, respectively, up to 38.16(1) and 45.45(1) T for Fe(1) and Fe(2) sites, respectively, at 16 K. This result could be attributed to the existence in this temperature range of some ferromagnetic contribution originated by a spin canting phenomenon (see Magnetic Behavior subsection). Below 16 K, the hyperfine field parameters are practically equal, 47.86(1) and 48.26(1) T for Fe(1) and Fe(2), respectively, and at 12 K both contributions almost overlap, as is observed in Figure 4. These results are in good agreement with an antiferromagnetic orientation of the practically equal magnetic moments corresponding to the $Fe(1)O_6$ and $Fe(2)O_6$ crystallographically independent sublattices.

ESR Spectroscopy. The ESR spectra performed at the X-band on a powdered sample exhibit isotropic signals centered at 3370 G (Figure 5). The value of $g = 2.00(1)$ is in good agreement with the presence of Fe^{3+} ions in octahedral coordination.[30] Thermal dependence of both line width and intensity show a slight increase between 290 and 110 K, the temperature below which the increase is more rapid due to a spin correlation in the case of the thermal evolution of the line width.[31] Both intensity and line width reach a maximum at 40 K and a minimum at 7 K from which they slightly increase again, probably due to an effect of the signal integration. The presence of a maximum and a minimum in the thermal evolution of the intensity and the line width can be caused by a spin canting or some kind of decompensation of the antiferromagneticaly aligned spins.

Specific Heat. The specific-heat data collected between 1.8 and 300 K are shown in Figure 6. The Cp curve shows a small peak (λ-type) at, approximately, 30 K, that indicates the establishment of a magnetic ordering at this temperature. At lower temperatures, we can notice another weak and broad peak at about 10 K. Above the magnetic transition, the continuous increase of the specific heat with increasing

(29) Menil, F. *J. Phys. Chem. Solids* **1985**, *46*, 763.

(30) Bencini, A.; Gatteschi, D. *EPR of exchange Coupled Systems*; Springer-Verlag: Berlin, 1990.

(31) Richards, P. M.; Salamon, M. B. *Phys. Rev. B* **1974**, *1*, 32.

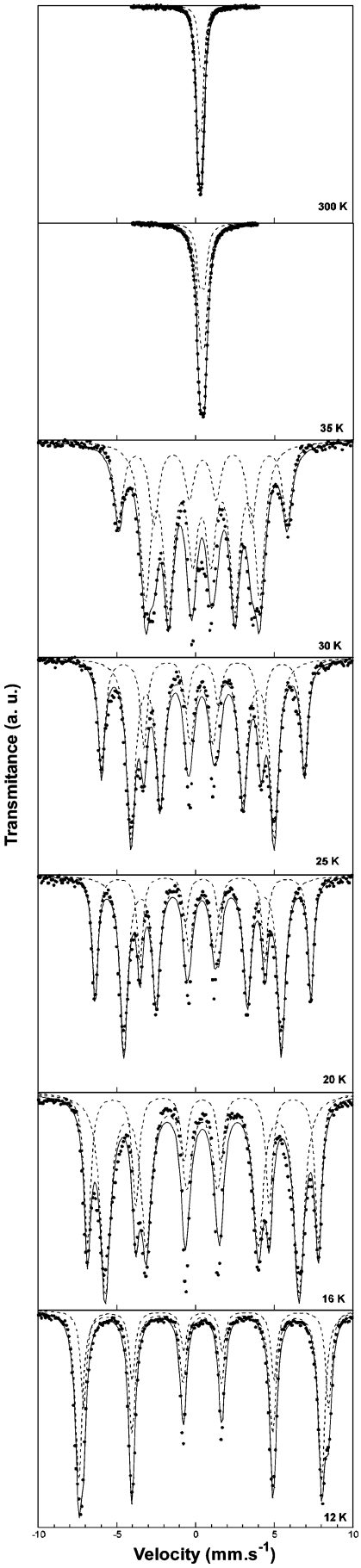

Figure 4. Mössbauer spectra from room temperature to 12 K.

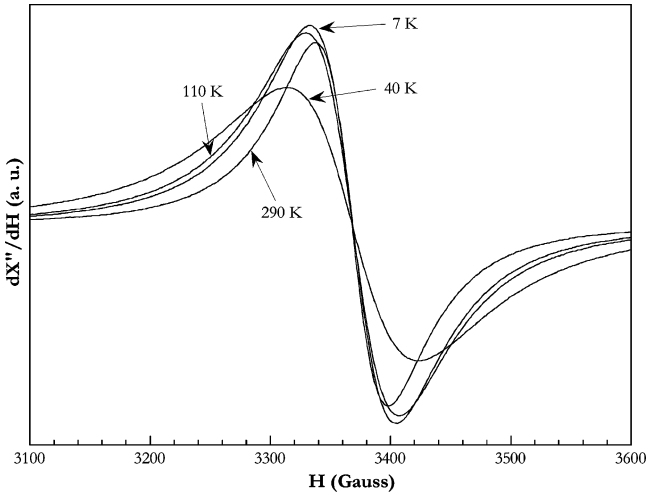

Figure 5. ESR signals for $(C_5H_{18}N_3)[Fe_3(HPO_3)_6]\cdot 3H_2O$ at different temperatures.

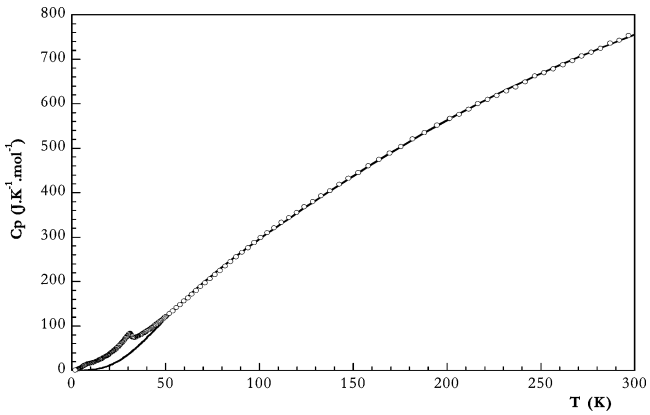

Figure 6. Thermal evolution of Cp and fit of the phononic contribution.

temperature is due to the lattice contribution (Cp_{pho}). The experimental data does not show saturation, probably due to the presence of light atoms such as the hydrogen ones in this phase, with very high excitation energy. This causes, at 300 K, the Cp value to be 775 J/mol K, smaller than the expected 1700 J/mol K, considering the Dulong and Petit law.[32] To estimate Cp_{pho}, the specific-heat data have been fitted to the Debye model, considering the existence of three different phonon spectra. In this way, if the number of atoms in the unit cell is n, we suppose n_1 atoms with a Debye temperature θ_1, n_2 atoms with a Debye temperature θ_2, and finally $n_3 = 68 - n_1 - n_2$ atoms with a Debye temperature θ_3, the total number of atoms in the chemical formula of the compound being 68. Taking into account that the hydrogen atoms are lighter than the other atoms in the compound, n_1 has been fixed as 30. So, in eq 1 there are four free parameters.

$$C_{pho}(T) = 30C_{pho}(\theta_{D1}) + n_2C_{pho}(\theta_{D2}) + (68 - 30 - n_2)C_{pho}(\theta_{D3}) \quad (1)$$

(32) Cheetham, A. K.; Day, P. *Solid State Chemistry. Techniques*, Oxford University Press: Oxford, 1991.

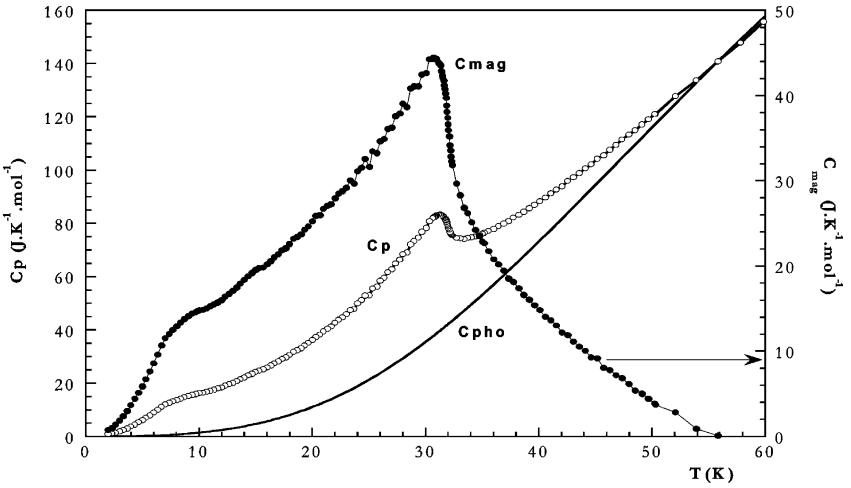

Figure 7. Thermal evolution of Cp, C_{phon}, and C_{mag}.

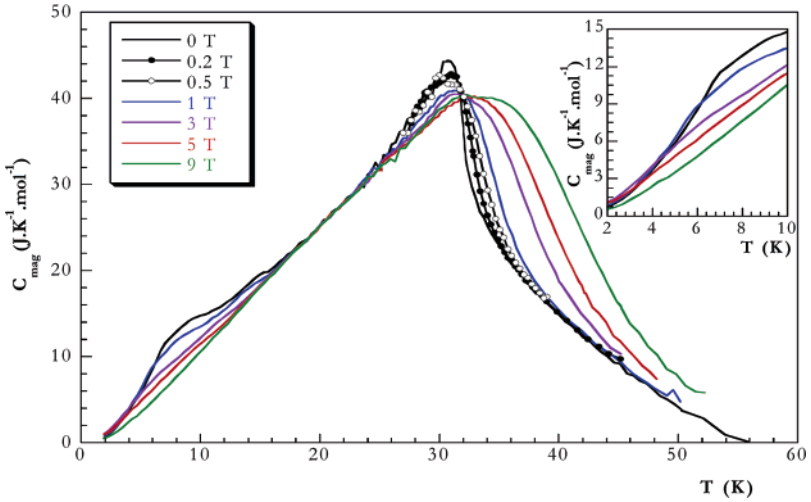

Figure 8. Specific-heat magnetic data under different magnetic fields. The inset shows the values of C_{mag} between 1 and 5 T.

where

$$C_{pho}(\theta_D) = 9R\left(\frac{T}{\theta_D}\right)^3 \int_0^{\frac{\theta_D}{T}} \frac{x^4 e^x \, dx}{(e^x - 1)^2}$$

The best fitting above the temperature of the λ-type peak, shown in Figure 7 as a solid line, is obtained from $\theta_{D1} = 3211$ K, $n_1 = 30$; $\theta_{D2} = 996$ K, $n_2 = 24.3$; and $\theta_{D3} = 272$ K, $n_3 = 13.7$.

The magnetic contribution was calculated as $Cp_{mag} = Cp - Cp_{pho}$ (Figure 7). In this figure a clear maximum at 30.7 K is observed. This indicates the existence of a three-dimensional magnetic ordering around this temperature. The ordering temperature is defined by the inflection point of $C_{mag}(T)$ above the maximum, in this case $T_c = 32$ K. The value of C_{mag} in the maximum is 44 J/mol K that corresponds to 14.7 J/mol K per iron atom. For temperatures below 32 K, we can observe an accident at 15 K, together with a weak and broad maximum at, approximately, 10 K. These irregularities in the thermal variation of Cp can be due to some change in the magnetic structure, probably due to a spin reorientation.

The magnetic contributions of Cp for all the magnetic fields applied have been calculated (Figure 8). We can see

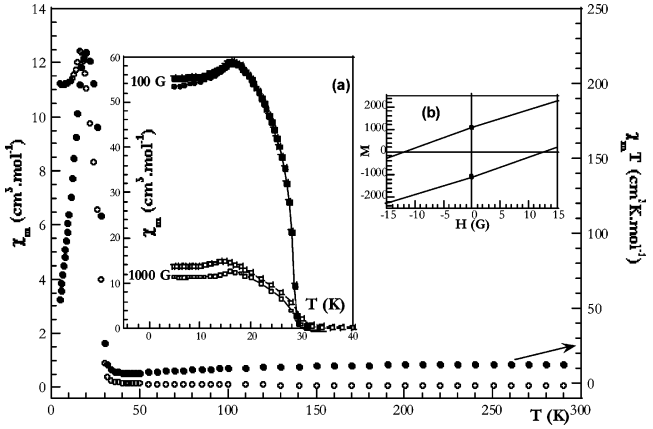

Figure 9. Thermal variation of χ_m and $\chi_m T$ at 1000 G. Inset a shows the magnetic susceptibility, χ_m, at 1000 and 100 G, and irreversibility of ZFC and FC curves. Inset b shows the magnetization (M) versus applied field (H) at 5 K.

that the magnetic field does not eliminate the λ-type peak, but this is to round off, and it is displaced at higher temperatures. This behavior is a characteristic of a ferromagnetic transition, probably due to a spin canting phenomenon.[33] The broad maximum of the C_{mag} versus T curve at 8

(33) Rawat, A.; Das, I. *Phys. Rev. B* **2001**, *64*, 52407.

K is affected below 15 K. In this region, the values of C_{mag} decrease whereas the magnetic field increases. However, in the lowest temperature region, the evolution between 1 and 5 T is the opposite: C_{mag} increases with increasing magnetic field, see inset of Figure 8. This behavior indicates that in this region the magnetic field transfers entropy from high to low temperatures, which is a characteristic of antiferromagnetic interactions.[34]

The entropy was calculated at different magnetic fields (see Supporting Information). At zero field, we notice a positive curvature up to, approximately, 10 K, with a practically linear increase up to T_c, a temperature at which the entropy takes negative curvature and maintains it at a constant. The value at saturation is 46 J/mol K, very close to the expected value (44.7 J/mol K) for three iron(III) cations with $S = {}^5/_2$. At the ordering temperature, the entropy is 40 J/mol K, which corresponds to the 80% of the maximum of the entropy of the system. This result indicates that the effects of short range order above T_c are small.[35] The magnetic field moves the entropy toward higher temperatures, maintaining the saturation value. This result is associated with ferromagnetic interactions.[36] However, the displacement in opposite directions in the region of low temperatures at fields lower than 5 T means that the predominant interactions in this region are antiferromagnetic in nature.[34]

Magnetic Behavior. Magnetic measurements were performed from room temperature to 5 K on a powdered sample. The thermal evolution of χ_m and $\chi_m T$ under an applied field of 1000 G is shown in Figure 9. The molar magnetic susceptibility follows the Curie−Weiss law [$\chi_m = C_m/(T - \theta)$] above ca. 170 K with values of Curie and Curie−Weiss constants of 13.92 cm^3 K·mol^{-1} and −25 K, respectively. At 30 K, the χ_m curve suddenly increases, reaching a maximum at 16 K while $\chi_m T$ smoothly decreases from 290 to 30 K, where it reaches a minimum. At this point, it shows a sudden increase reaching a maximum at 20 K. Zero field cooling and field cooling magnetic susceptibilities, measured under applied fields of 1000 and 100 G, show irreversibility below 32 K. Measurements performed under an applied field of 100 G show higher susceptibility values than those under 1000 G (see inset a in Figure 9). This effect is due to the system of antiferromagnetic interactions over the whole temperature range where the sudden increase of the $\chi_m T$ curve is caused by a weak ferromagnetism phenomenon.

Hysteresis observed in magnetization versus magnetic field measurements at 5 K (see inset b in Figure 9) corroborates a ferromagnetic component at this temperature, with values of remnant magnetization and coercitive field of 1090 emu·mol^{-1} and 12 G, respectively, in a predominantly antiferromagnetic system. The magnetization value at highest field of 36500 emu·mol^{-1}, significantly lower than the value for three iron(III) cations present in the formula of 83785 emu·mol^{-1}, is further evidence for antiferromagnetic order.

The remnant magnetization versus temperature measurement shows two transition temperatures of 30 and 16 K, which correspond to a three-dimensional magnetic ordering and to a possible spin reorientation, respectively, in good agreement with the specific heat results.

Acknowledgment. This work has been financially supported by the "Ministerio de Educación y Ciencia" (MAT2004-02071), the "Universidad del País Vasco" (UPV/EHU) (9/UPV00130.310-16967/2004 and 9/UPV00169.310-13494/2001), and the "Fondo Europeo de Desarrollo Regional". We thank Dr. J. P. Chapman and Dr. I. Orue ("Fondo Europeo Social" and "Ministerio de Ciencia y Tecnología") for the X-ray diffraction and magnetic measurements, respectively. U-Chan Chung thanks the UPV/EHU for funding.

Supporting Information Available: Crystallographic data in CIF format; atomic coordinates and equivalent temperature factors; and additional spectra. This material is available free of charge via the Internet at http://pubs.acs.org.

IC060815U

(34) Dan'kov, S.-Y.; Tishin, A. M.; Pecharsky, V. K.; Gschneidner, K. A. *Phys Rev B* **1998**, *57*, 3478.
(35) Chung, E. M. L.; Lees, M. R., McIntyre, G. J.; Wilkinson, C.; Balakrishnan, G.; Hague, P. J.; Visser, D.; Mck Paul, D. *J. Phys.: Condens. Matter* **2004**, *16*, 7837.
(36) Tishin, A. M.; Gschneidner, K. A.; Pecharsky, V. K. *Phys. Rev. B* **1999**, *59*, 503.